Interfacial structural transition in hydration shells of a polarizable solute

Mohammadhasan Dinpajooh and Dmitry V. Matyushov
*Department of Physics and Department of Chemistry & Biochemistry, Arizona State University, PO Box 871504, Tempe, Arizona 85287**

Electrostatics of polar solvation is typically described by harmonic free energy functionals. Polarizability contributes a negative polarization term that can make the harmonic free energy negative. The harmonic truncation fails in this regime. Simulations of polarizable ideal dipoles in water show that water's susceptibility passes through a maximum in the range of polarizabilities zeroing the harmonic term out. The microscopic origin of the non-monotonic behavior is an interfacial structural transition involving the density collapse of the first hydration layer and enhanced number of dangling OH bonds.

PACS numbers: 61.20.Ja, 61.25.Em, 68.18.Jk, 68.08.Bc, 82.60.Qr

When the electric field $\mathbf{E}_0$ is introduced by a solute into a condensed polar material, the response of the medium (solvent) is largely linear: the electrostatic potential or field of the solvent is a linear function of solute's charge or dipole. The linear response (also known as the Gaussian approximation) assumes a harmonic free energy as a function of the medium collective coordinate coupled to $\mathbf{E}_0$ [1]. In polar solvents, the dipolar polarization density of the solvent $\mathbf{P}$ becomes such collective coordinate when higher-order multipolar fields, such as the quadrupolar polarization density, are neglected [2]. The harmonic electrostatic free energy of the solution reads

$$\mathcal{F}[\mathbf{P}] = -\mathbf{E}_0 * \mathbf{P} + (2\chi)^{-1}\mathbf{P} * \mathbf{P}, \qquad (1)$$

where the asterisk implies both the tensor contraction and the volume integration over the space occupied by the solvent [3]. The solvation susceptibility χ is an analog of the susceptibility of a material to an external field, but it also depends on the geometry of the solute repulsive core. This dependence enters through the Maxwell boundary conditions when $\mathbf{P}$ is approximated by a continuum polarization field.

The minimization of $\mathcal{F}[\mathbf{P}]$ in respect to $\mathbf{P}$ yields the equilibrium solvation free energy $F_0 = -(\chi/2)\mathbf{E}_0 * \mathbf{E}_0$, which becomes the standard Born equation for a spherical ion when the longitudinal susceptibility $\chi^L \propto (1 - \epsilon^{-1})$ is used in Eq. (1). Since the solvent dielectric constant ϵ is large for many polar solvents, F_0 is close to its saturation limit at $\epsilon \to \infty$. Only minor changes in the solvation free energy can be achieved by changing either the solvent or the thermodynamic state of the solution.

The situation can potentially change near the critical point of the phase diagram where the second, harmonic term in Eq. (1) vanishes [4]. This term describes the reversible work (free energy) required to change the polarization of the liquid from $\mathbf{P} = 0$ to $\mathbf{P}$ when the solute produces no field ($\mathbf{E}_0 = 0$). Correspondingly, a large quadratic penalty for increasing the polarization makes strong variations of F_0 hard to achieve. The general question we address here is whether one can significantly reduce the quadratic penalty and what kind of solvent response might be expected if the quadratic term in the free energy functional approaches zero, which corresponds to $\chi \to \infty$.

Using the analogy with bulk phase transitions [4], we consider here a specific physical mechanism of reaching a state of vanishing harmonic expansion term. The molecular polarizability of the solute is used to tune the harmonic response. In order to simplify the electrostatic part of the problem, the solute is a dipole $\mathbf{m}$ at the center of a spherical core characterized by the isotropic dipolar polarizability α. The electrostatic problem can be recast in terms of the instantaneous field E, which is the projection of the electric field of the solvent on the solute dipole

$$\mathcal{F}[E] = -mE + (\kappa/2)E^2 - (\alpha/2)E^2 + G[E]. \qquad (2)$$

Similarly to Eq. (1), the second term in this equation is the harmonic free energy penalty for producing an electric field inside the solute carrying no dipole and no polarizability. The "spring constant" $\kappa \propto \chi^{-1}$ carries the meaning of the solvation modulus; $\kappa^{-1} = (2/R^3)(\epsilon - 1)/(2\epsilon + 1)$ for a spherical dipole in a dielectric [5]. The third term is the free energy of polarizing the polarizable solute, and $G[E]$ includes the higher-order expansion terms.

It is clear from Eq. (2) that the harmonic term vanishes at $\kappa = \alpha$. The harmonic truncation becomes inadequate in the vicinity of this point and higher-order expansion terms, given by $G[E]$, are needed. A general form of $G[E]$ is, however, unknown. Therefore, numerical Monte Carlo (MC) simulations are used here to study the vicinity of the critical point $\kappa = \alpha$ and the transition to non-harmonic solvation when the harmonic truncation in Eqs. (1) and (2) becomes inapplicable. The questions addressed here are whether one can achieve a stronger solvent response near $\kappa = \alpha$ compared to the standard harmonic (Gaussian) models and whether microscopic changes in the structure of the interface are realized near the critical point.

The answers to both these questions are affirmative. Figures 1 and 2 illustrate our main findings. Figure 1

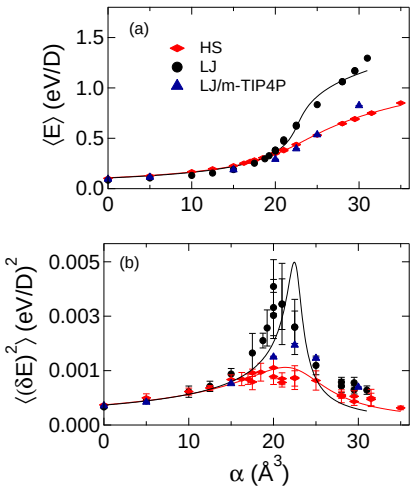

FIG. 1. (a) Onsager reaction field [5] $\langle E\rangle$ for the hard-sphere (HS) and Lennard-Jones (LJ) solutes with the dipole moment $m_0 = 5$ D and varying polarizability in TIP3P water at $T = 298$ K [6]. The solid lines are fits to the Landau functional in E; simulation errors are smaller than symbol sizes. (b) The variance of E with error bars indicating the simulation uncertainties. The solid lines refer to the Landau theory based on the fitting of $\langle E\rangle$ shown in (a). The blue triangles indicate the results of molecular dynamics simulations for the LJ solute in modified TIP4P water [6] (see SM).

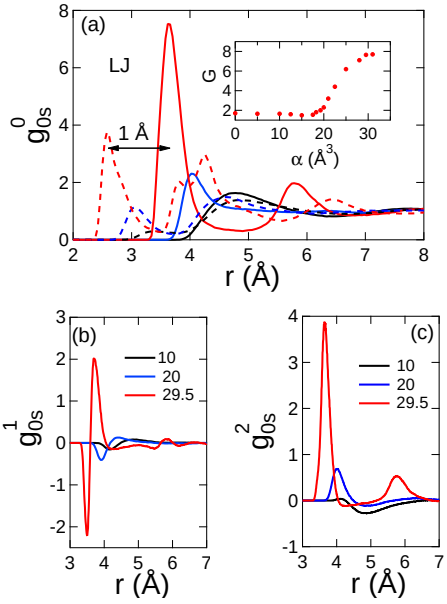

FIG. 2. Solute-water distribution functions $g^{\ell}_{0s}(r)$ (Eq. (3)) for the LJ solutes with the polarizabilities α indicated in the plot. (a) The solute-oxygen (solid lines) and solute-hydrogen (dashed lines) radial distribution functions ($\ell = 0$). The inset shows the height of the first solute-solvent peak G. The horizontal arrow indicates the separation of the first oxygen and hydrogen peaks. The orientational functions with $\ell = 1$ and $\ell = 2$ are shown in panels (b) and (c), respectively.

shows the average field at the solute dipole (Onsager's reaction field [5]) and the variance of the solvent electric field, both as functions of the solute polarizability. We observe an inflection of the average field at $\alpha^* \simeq 20 - 22$ Å^3 (Fig. 1a) and a corresponding spike in the field variance (Fig. 1b). The field variance is proportional to the dipolar susceptibility and the spike in the variance implies a corresponding spike in the susceptibility. The divergence $\chi \to \infty$ is avoided by the higher-order expansion terms in $G[E]$ as discussed below. We start the discussion with the question of the microscopic origin of the susceptibility spike. We have found that it is driven by a structural transition of the hydration shell.

The MC simulations reported here were done for two solutes: a hard-sphere (HS) solute with the HS radius $R_{\rm HS} = 4.15$ Å and a Lennard-Jones (LJ) solute with the LJ radius $R_{\rm LJ} = 3$ Å. Each solute carried two opposite charges, $+q$ and $-q$, placed symmetrically relative to the solute center at the short distance of $d = 0.05$ Å to model an ideal dipole. The LJ solute additionally had a LJ 12–6 site located at its center with the LJ energy $\epsilon_{\rm LJ} = 280$ K. The dipole moment of the solute was varied by changing the magnitude of q (see Supplemental Material (SM) for the details of the simulation protocol). Most of the results are reported for TIP3P water [6]. Our conclusions are not sensitive to the choice of either the water model or specifics of the solute. This is indicated by the comparison with the results obtained with a slightly modified TIP4P water model [6] (Fig. 1) combined with a larger distance between opposite charges in the solute ($d = 1.5$ Å).

The reason for choosing two solutes was to show that the general phenomenology reported here is not a property of some specific solute-solvent interaction potential, but instead reflects a more general competition between the free energy gain of polarizing the solute and the free energy penalty of orienting the solvent dipoles to create the electric field. Two different solute sizes were adjusted to produce nearly equal polar response of TIP3P water to the solute dipole. The reaction field is a linear function of m at $\alpha = 0$: $\langle E\rangle = \kappa^{-1} m$. The sizes of HS and LJ solutes were therefore chosen to produce close values of κ in two cases ($\kappa_{\rm HS} = 28.7$ Å^3 and $\kappa_{\rm LJ} = 29.6$ Å^3, see Fig. S1 in SM).

Figure 2 illustrates the structure of the hydration shell of the polarizable LJ solute as defined by the orientational solute-solvent distribution functions $g^{\ell}_{0s}(r)$ of increasing order ($g^{\ell}_{0s}(r)$ of the HS solute are shown in Fig. S2 in SM). The function $g^{\ell}_{0s}(r)$ is given as the average Legendre polynomial of order ℓ specified by the scalar product of the unit dipole moment $\hat{\mathbf{m}}_j$ and the radial unit vector $\hat{\mathbf{r}}_j$ of the water molecule j positioned at distance r_j from the solute center

$$g^{\ell}_{0s}(r) = \rho^{-1} \sum_j \langle P_\ell(\hat{\mathbf{m}}_j \cdot \hat{\mathbf{r}}_j)\delta(\mathbf{r}_j - \mathbf{r})\rangle \,. \qquad (3)$$

Here, ρ is the number density of bulk water.

The orientational structure of interfacial water next to HS and LJ solutes is consistent with the phenomenology established for planar hydrophobic surfaces [7], molecular non-polar solutes [8], and hydrated nanoparticles [9] when α is small. The height of the first maximum G of the solute-water radial distribution function ($\ell = 0$) is below the maximum of bulk water (inset in Fig. 1a), indicating a weak dewetting of the interface [10]. In addition, the water dipoles are preferentially oriented tangentially to the dividing surface [7]. The increase of the solute polarizability dramatically changes this phenomenology, producing a structural transition in the hydration shell. Unlike the gradual change to the hydrophilic behavior caused by increasing surface polarity [11], the transition observed here is abrupt and analogous to the global loss of stability at the point of phase transition [4].

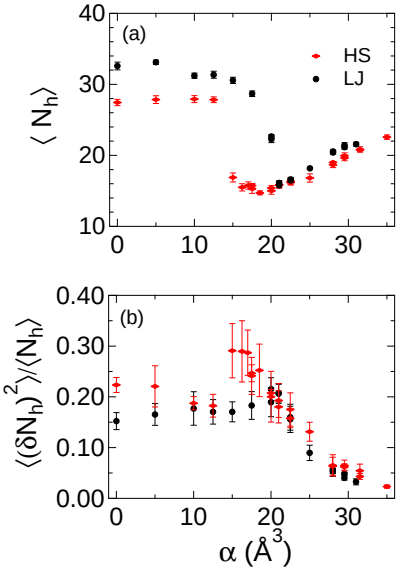

FIG. 3. (a) The average numbers of water molecules in the first hydration shell of HS and LJ solutes. (b) Hydration shell compressibilities [12]. The error bars indicate the simulation uncertainties.

Increasing the solute polarizability substantially alters the density profile ($\ell = 0$) and the orientational structure ($\ell > 0$) of the hydration shell. One clearly sees an increase in the density of the first hydration layer (Fig. 2a): the maximum of the radial distribution function grows with increasing polarizability and the first minimum decreases in amplitude and becomes increasingly shallow. Near the critical polarizability α^*, producing the spike in the electric field variance (Fig. 1b), a layering transition [13] occurs separating the first and the second hydration layers. This transition is particularly distinct for the HS solute (Fig. S2 in SM).

Collapse of the first hydration layer is also seen as a stepwise drop in the number of hydration waters N_h (Fig. 3a) calculated within the shell geometrically defined to extend up to the first minimum of the radial distribution function. The variance of the number of shell waters drops, however, faster than the average with increasing α, resulting in an overall decrease of the shell compressibility [12] $\langle(\delta N_h)^2\rangle/\langle N_h\rangle$ at $\alpha > \alpha^*$ (Fig. 3b). The structural collapse of the hydration layer is accompanied by an orientational transition to accommodate the high density of the first-shell waters.

The first peak of the solute-hydrogen distribution function shifts, with increasing α, to shorter distances compared to the first solute-oxygen peak (Fig. 1a). This shift indicates the switch of the preferential outward (into water) orientation of the interfacial hydrogens to the inward orientation (toward the solute). In the range of $\alpha > \alpha^*$, the distance between the oxygen and hydrogen peaks is $\simeq 1$ Å, essentially equal to the O-H distance in TIP3P water. This implies that the corresponding OH bonds are protruding from water toward the solute, thus forming "dangling " OH bonds [14, 15].

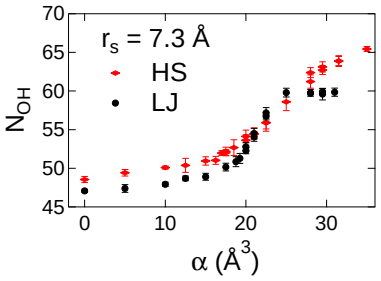

FIG. 4. The number of unsatisfied hydrogen bonds [16] $N_{\rm OH}$ within the sphere of radius $r_s = 7.3$ Å measured from the center of HS and LJ solutes.

The appearance of dangling bonds seen from the radial distribution functions is consistent with the growth of a positive first peak of the orientational distribution $g^2_{0s}(r)$ in Fig. 2c. It is also clear that the release of dangling OH eliminates the restrictions imposed by the bulk-like tetrahedral arrangement of the water molecules and, therefore, allows the collapse of the hydration layer to a higher density. The result is a distinct structural transition releasing dangling OH bonds and occurring at the critical value of the solute polarizability zeroing out the quadratic term in the free energy functional. The number of dangling OH bonds can be viewed as an order parameter of the structural interfacial transition, which can be experimentally monitored [14, 15].

The dangling bonds are identified experimentally by their separate vibrational line [14]. There is no clear connection between this spectroscopic identification and structural information available from simulations [15]. Since we cannot directly count spectroscopically active dangling bonds, we have calculated unsatisfied hydrogen bonds according to Wernet *et al* [16]. The numbers of unsatisfied bonds are typically higher [15] than spec-

troscopic dangling OH: about one dangling OH per four water molecules at extended hydrophobic interfaces [14] or even lower numbers around molecular-sized solutes [15]. Nevertheless, the numbers of unsatisfied bonds vs α might mirror the corresponding trend for dangling bonds. Those numbers indeed increase with α when counted in water layers of different thickness. Figure 4 shows the results for the closest hydration layer with the thickness of the water diameter. A similar trend is seen for a wider shell (Fig. S3 in SM).

The simulation data for the reaction field were fitted (solid lines in Fig. 1a) by applying a Landau functional [4] involving the fourth and sixth order expansion terms in $G[E]$ in Eq. (2): $G[E] = -(b/4)E^4 + (c/6)E^6$. The exclusion of the odd powers in E is required by the invariance under the inversion $E \to -E$ (coordinates inversion) when $m = 0$. The fit to the reaction field from simulations is then used to calculate the variance of E as the second derivative of $\mathcal{F}(E)$: $\langle(\delta E)^2\rangle = [(\partial^2\mathcal{F}/\partial E^2)|_{E=0}]^{-1}$. The results of these calculations are shown by the solid lines in Fig. 1b. We also find that the spike in $\langle(\delta E)^2\rangle$ does not produce a non-monotonic dependence of the overall solvation free energy on α: $F_0(\alpha)$ is significantly steeper at $\alpha > \alpha^*$, but the overall dependence is still monotonic (Fig. S4 in SM).

Several systems and observables can display the phenomenology reported by our simulations. The first two moments of the solvent electric field largely determine the shift and inhomogeneous line width of optical dyes. The non-monotonic behavior of the field variance vs α should therefore be mirrored by the spectral width. The overall line-shape can be calculated from the Landau functional $\mathcal{F}(E)$, which extends the harmonic theory of spectroscopy of polarizable chromophores [17] to non-harmonic solvation.

Non-harmonic solvation can be anticipated for several systems. For instance, the polarizability of a semiconductor nanoparticle scales as the fourth power of its radius, $\alpha \propto R^4$. The proportionality coefficient can be very high: $\alpha \simeq 0.08\text{Å}^3(R/\text{Å})^4$ has been reported for photoexcited CdSe nanoparticles in the range of radii 1–2.5 nm [18]. From a general scaling perspective, $\kappa \propto R^3$ for dipolar solutes in Eq. (2) [5] (Fig. S1 in SM). With $\alpha \propto R^4$, there is always a critical size at which the transition to non-harmonic solvation should occur. When the values of κ obtained in our simulations are rescaled to nanoparticle sizes used in Ref. 18 we find them to fall in the regime of non-harmonic solvation, $\kappa < \alpha$. Similar arguments apply to organic ionic solutes (such as tetraalkylammonium cations studied in Ref. 15). The force constant scales as $\kappa \propto R$ for spherical ions, while the polarizability of many organic molecules scales as R^3. The transition to non-harmonic solvation, and the related structural transition of the hydration layer, can be predicted for this configuration as well.

In summary, we have discovered a structural density collapse of the hydration shell promoted by the negative free energy of polarizing a polarizable solute. The density collapse induces a concomitant orientational transition of the hydration shell dipoles toward the inward orientation. Both transitions are manifested in an increase in the density of dangling OH bonds which have been viewed as potential catalytic centers to promote heterogeneous catalysis [20]. Our picture is distinct from the traditional "iceberg model" anticipating enhanced structuring of water around a non-polar solute [21]. In contrast, high polarizability breaks the bulk-like water structure creating a high density of surface OH defects. The crossover is abrupt since it is caused by zeroing of the quadratic term in the solvation free energy, analogous to the point of criticality in bulk phase transitions.

This research is supported by the NSF (CHE-1213288) and through XSEDE (TG-MCB080116N).

* dmitrym@asu.edu

[1] G. Hummer, L. R. Pratt, and A. E. Garcia, J. Phys. Chem. **100**, 1206 (1996).
[2] J. D. Jackson, *Classical Electrodynamics* (Wiley, New York, 1999).
[3] B. U. Felderhof, J. Chem. Phys. **67**, 493 (1977).
[4] H. E. Stanley, *Introduction to phase transitions and critical phenomena* (Oxford University Press, New York, 1987).
[5] L. Onsager, J. Am. Chem. Soc. **58**, 1486 (1936).
[6] W. L. Jorgensen *et al.*, J. Chem. Phys. **79**, 926 (1983).
[7] C. Y. Lee, J. A. McCammon, and P. J. Rossky, J. Chem. Phys. **80**, 4448 (1984).
[8] D. M. Huang and D. Chandler, Phys. Rev. E **61**, 1501 (2000).
[9] C. D. Daub, D. Bratko, T. Ali, and A. Luzar, Phys. Rev. Lett. **103**, 207801 (2009).
[10] S. Garde *et al.*, Phys. Rev. Lett. **77**, 4966 (1996).
[11] N. Giovambattista, P. G. Debenedetti, and P. J. Rossky, J. Phys. Chem. B **111**, 9581 (2007).
[12] S. Sarupria and S. Garde, Phys. Rev. Lett. **103**, 037803 (2009).
[13] I. Brovchenko and A. Oleinikova, *Interfacial and confined water* (Elsevier, Amsterdam, 2008).
[14] Q. Du, R. Superfine, E. Freysz, and Y. R. Shen, Phys. Rev. Lett. **70**, 2313 (1993).
[15] J. G. Davis *et al.*, Nat. Chem. **5**, 796 (2013).
[16] P. Wernet *et al.*, Science **304**, 995 (2004).
[17] D. V. Matyushov, J. Chem. Phys. **115**, 8933 (2001).
[18] F. Wang *et al.*, Nat. Mater. **5**, 861 (2006).
[19] C. S. Tian and Y. R. Shen, Proc. Natl. Acad. Sci. USA **106**, 15148 (2009).
[20] Y. Jung and R. A. Marcus, J. Phys.: Condens. Matter **22**, 284117 (2010).
[21] H. S. Frank and M. W. Evans, J. Chem. Phys. **13**, 507 (1945).